# Flow Field Study of Bio-Inspired Corrugated Airfoils at Low Reynolds Number with Different Peak Shapes

Y. D. DWIVEDI*

*Corresponding author
Department of Aeronautical Engineering, Institute of Aeronautical Engineering, Dundigal, Hyderabad, 500043, Telangana, India,
yddwivedi@gmail.com

DOI: 10.13111/2066-8201.2020.12.3.7

*Received: 12 April 2020/ Accepted: 22 July 2020/ Published: September 2020*


***Abstract:*** *This study is intended to understand the fluid flow behaviour of a bio inspired corrugated wing obtained from the mid span of the dragonfly wing with different peak shapes of the corrugations. The aerodynamic effect due to variation of the shape of the first peak is studied with triangular and a curved peak shapes. The coordinates of the corrugated wing of the dragonfly were obtained from the existing literature and scaled up 1:50 to do the computational work on it. The corrugated wing was modeled by using a modeling software, the meshing was done by using ICEMCFD with a rectangular block meshing and simulated in Ansys Fluent software at 35000 Reynolds number and angles of attack ranging from 4° to 12°. The k-ε turbulence modeling was deployed to capture turbulence in the tested domain. The boundary conditions and size of the domain were selected as per available experimental wind tunnel setup. The flow characteristics like pressure and velocity of the triangular and curved peaks were obtained computationally and compared with each other having same geometrical parameters. The simulated results showed that the curved peak performed aerodynamically better than the triangular peak. The leading edge vortices were observed in both models trapped in the trough of the first valley with some different intensity. The validation of the computational flow results was done by existing experimental flow visualization in a wind tunnel and both results agree with each other.*

***Key Words:*** *Corrugated wing, Leading edge vortices, k-ε turbulence modeling, Bio-inspired corrugation, Smoke flow visualization*

## 1. INTRODUCTION

All the insects' wings of natural low Reynolds number (Re) fliers are not smooth even if the wings have well defined and fine-tuned pleats which were optimized after millions of years of their evolution. These pleats are called corrugations and can be found on many fliers like dragonflies, hoverflies, etc and aquatic animals like crocodiles and sharks, etc. Most of the insects have mainly two types of flight modes; the first one is the more dominated flapping mode and the second one is the gliding mode used to preserve the energy. The dragonfly is one of the unique insects, which can perform considerably high maneuvers, sharp climbs and hover in all unfavorable climatic conditions. The dragonfly (*Pantala flavescen*) is able to aloft for 10-15 seconds at a speed about 15 $ms^{-1}$ [1]. Another dragonfly *Aeshna genus* is able to glide for 30 seconds without appreciable loss in altitude [2]. Another study on Nannophya pygmaea (*Anisoptera: Libellulidae*) found that the gliding endurance can last for 0.5 seconds, with range of 1m and sinking rate of 2.5 $ms^{-1}$ [3]. The typical range of Re for dragonfly vary

from 100 to 10000 [3]. However, the micro aerial vehicles (MAVs) can fly with a maximum speed of 15 $ms^{-1}$ with a maximum span of 0.15 m, which gives the maximum Re $10^5$.

The wings of the dragonfly are well-defined and tuned corrugations, where the corrugation patterns vary in both spanwise and chordwise direction [4]. The mechanical properties of the wing structure vary throughout the wing and the factors which affect these properties are the depth of the pleat, peak shapes, and rigidity of the cross veins [5]. Experimental analysis of the corrugated wings of the dragonfly were conducted and concluded that the corrugation on the wing does not improve significantly the aerodynamic performance [6], [7], [8], [9], [10]. However, Rudolph [10] has shown that the pleats are able to delay the flow separation and improve in stall angle considerably. The aerodynamic lift of the pleated airfoil was found better than the conventional airfoil at Re 1500 [11]. A filming test also shown the lift coefficient enhancement from 0.93 to 1.07 due to pleats of the dragonfly wings during glide at Re 700 and 2400 [12], [13] and [14]. A wind tunnel study was performed at Re $1.1x10^4$ and $1.5x10^4$ to understand the effect of camber, maximum thickness and leading edge sharpness and concluded that the sharper leading edge performed better [15]. A flow visualization study [16] notices that the leading edge vortices (LEV) were trapped and play a major role in changing the effective profile and concluded that the pleats present in the dragonfly wing preserve the trapped vortices in the valley, which makes the pleats to behave like a profiled airfoil. Computational studies [17], and [18] have demonstrated a better aerodynamic performance of the corrugated airfoil than the profiled one in gliding condition at low Re. Few recent studies [19], [20], [21] have measured the boundary layers experimentally and numerically and observed that pleats of the wing delay the stall and flow separation, significantly. The boundary layers of the pleated wing were found thinner than the tested flat plate of the same geometric and flow conditions.

There are numerous studies about computational and experimental flow visualization over the dragonfly wings which showed the existence of LEVs on the upper surface of the wings [22], [23], [24], [25]. Some more studies were performed to understand the aerodynamic behaviour of bio-inspired corrugated wing with different Re [26], [27], [28] and observed that the bio inspired wings produce a better aerodynamic performance at low Re regimes. The parametric study by Levy and Seifert [29], [30] & [31] have shown that the variation of the wing geometry, affected the aerodynamic behaviour of the wing.

In this paper, the aerodynamic characteristics and fluid flow behavior of the dragonfly forewing mid span are carried out at the Re 35000 by altering the first peak shape. The "profile 2" from the Kesel [16] is taken as baseline triangular first peak with horizontal orientation of the leading edge. The Re of 35000 was selected as the micro aerial vehicles (MAVs) fly in this range. The aim of this study is to assess the aerodynamic performance of the curved first peak (model 2) of a corrugated airfoil and to compare it with the triangular first peak (model 1) from [16]. This study is intended to assess the possibility of using these types of wings in future micro aerial vehicles wings.

## 2. METHODOLOGY

### 2.1 Governing Equations

The equations governing the flow in the numerical solver are the steady, viscous incompressible Navier–Stokes equations. The non-dimensional momentum and continuity equations are as follows:

$$\frac{\partial u_i}{\partial x_i} = 0 \tag{1}$$

$$\frac{\partial u_i u_j}{\partial x_j} = -\frac{\partial p}{\partial x_i} + \frac{1}{Re}\frac{\partial^2 u_i}{\partial x_j x_j} \tag{2}$$

The equations are non-dimensionalized with the appropriate length and velocity scales, in this case the airfoil chord and free stream velocity. Here Re corresponds to the Reynolds number which is defined as:

$$Re = \frac{\rho u_\infty c}{\mu} \tag{3}$$

The important aerodynamic characteristics examined are the lift coefficient ($C_L$), drag coefficient ($C_D$) and the gliding ratio which are defined as:
Lift Coefficient is given by

$$C_L = \frac{L}{0.5\rho u_\infty^2 c} \tag{4}$$

Drag Coefficient is given by

$$C_D = \frac{D}{0.5\rho u_\infty^2 c} \tag{5}$$

Gliding Ratio:

$$G = \frac{C_L}{C_D} \tag{6}$$

### 2.2 Numerical Modeling

#### 2.2.1. Airfoil Geometries

A corrugated airfoil with triangular first peak known as model 1 as shown in Fig. 1 and another corrugated airfoil with curved first peak with radius 1 mm known as model 2 as shown in Fig. 2, were modeled using ANSYS workbench software with suitable co-ordinates to test their performance in gliding flight. The chord length of both profiles was taken the same, 52 mm. These two different types of models were computationally evaluated and compared with each other. Both models have the same geometric parameters except for the shape of the first peak i.e. model 1 has a triangular peak and model 2 has a curved peak of 1 mm radius.

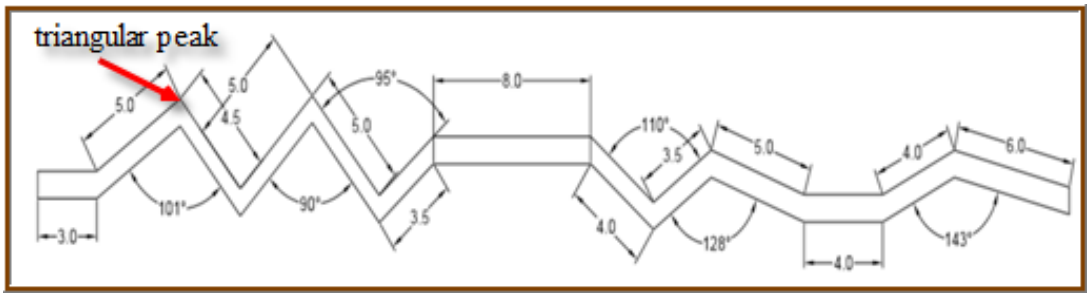


Figure 1. Geometry of corrugated airfoil with triangular first peak [16]: model 1

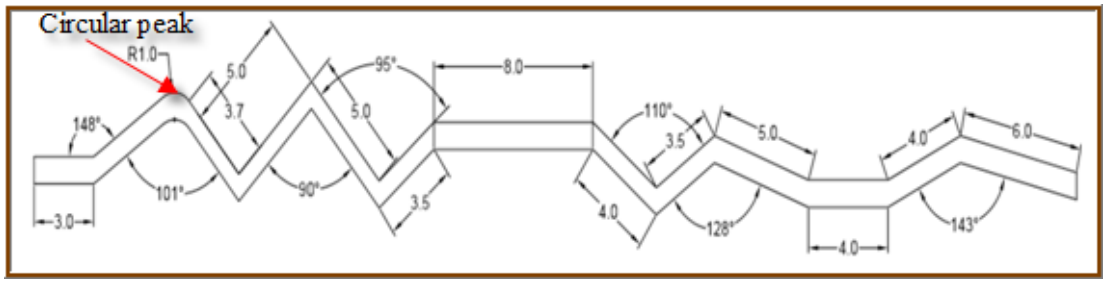


Figure 2. Geometry of corrugated airfoil with curved first peak [20]: model 2

### 2.2.2 Computational grid and boundary conditions

Computational grid used for the simulations is shown in Fig. 3. The free stream velocity, and the static pressure are prescribed at the inlet.

The distance between the top and the bottom boundaries is taken as 600 mm which is the width of the wind tunnel where the physical models are being tested. ICEMCFD is used for meshing the grid.

Blocking structured meshing technique is used for generating a structured mesh suitable for these cases.

A grid convergence test is carried out on one of the corrugated models i.e., model 1 to fix the smallest element size near the airfoil wall as well as the total number of elements required.

The geometric model is shown in Fig. 1 upon which the grid independence test is carried out. Results show convergences for boundary element size of 0.5 mm and below near the airfoil boundary.

The solution convergence of the simulation of a corrugated profile is shown in Fig. 5 and the mesh independence or grid convergence results are plotted in Fig. 6.

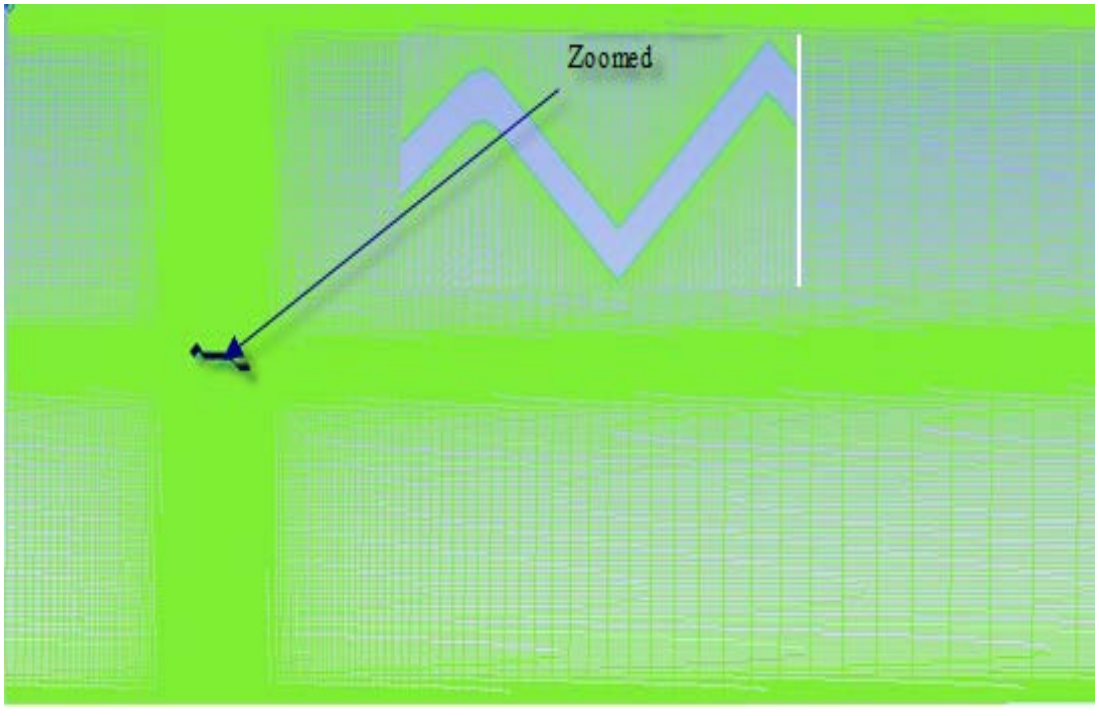


Figure 3. Computational Grid on triangular peak model 1 corrugated airfoil

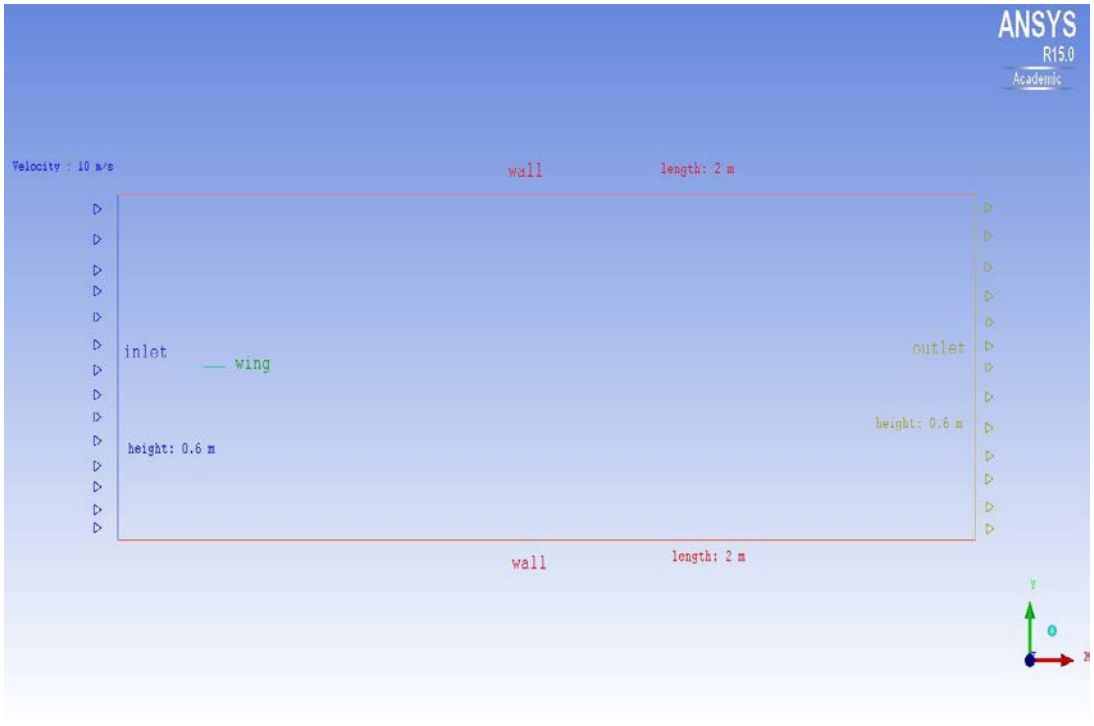


Figure 4. Computational domain of triangular peak model 1 airfoil

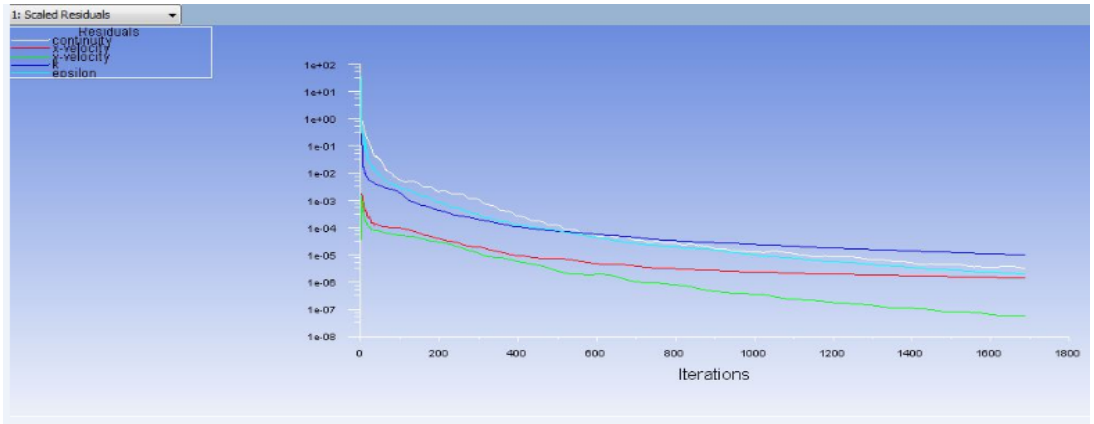


```
  1672  3.5088e-06  1.4495e-06  6.0474e-08  1.0180e-05  2.0338e-06  0:01:27  328
  iter  continuity  x-velocity  y-velocity          k     epsilon     time/iter
  1673  3.4901e-06  1.4485e-06  6.0121e-08  1.0167e-05  2.0257e-06  0:02:15  327
  1674  3.4674e-06  1.4474e-06  6.0233e-08  1.0155e-05  2.0225e-06  0:01:47  326
  1675  3.4484e-06  1.4464e-06  5.9882e-08  1.0142e-05  2.0145e-06  0:01:26  325
  1676  3.4256e-06  1.4454e-06  5.9998e-08  1.0129e-05  2.0115e-06  0:02:13  324
  1677  3.4066e-06  1.4444e-06  5.9663e-08  1.0117e-05  2.0035e-06  0:01:46  323
  1678  3.3847e-06  1.4433e-06  5.9780e-08  1.0104e-05  2.0005e-06  0:02:29  322
  1679  3.3667e-06  1.4424e-06  5.9438e-08  1.0092e-05  1.9927e-06  0:01:59  321
  1680  3.3455e-06  1.4414e-06  5.9557e-08  1.0080e-05  1.9897e-06  0:01:35  320
  1681  3.3281e-06  1.4405e-06  5.9212e-08  1.0067e-05  1.9820e-06  0:02:19  319
  1682  3.3066e-06  1.4395e-06  5.9317e-08  1.0055e-05  1.9791e-06  0:01:51  318
  1683  3.2885e-06  1.4386e-06  5.8976e-08  1.0043e-05  1.9716e-06  0:01:29  317
  iter  continuity  x-velocity  y-velocity          k     epsilon     time/iter
  1684  3.2707e-06  1.4377e-06  5.9079e-08  1.0031e-05  1.9688e-06  0:02:14  316
  1685  3.2569e-06  1.4368e-06  5.8726e-08  1.0019e-05  1.9615e-06  0:01:47  315
  1686  3.2394e-06  1.4358e-06  5.8812e-08  1.0006e-05  1.9586e-06  0:01:25  314
! 1687 solution is converged
  1687  3.2264e-06  1.4350e-06  5.8459e-08  9.9944e-06  1.9516e-06  0:02:11  313
```

Figure 5. Convergence test for curved peak wing model 1 at 4 degree AOA

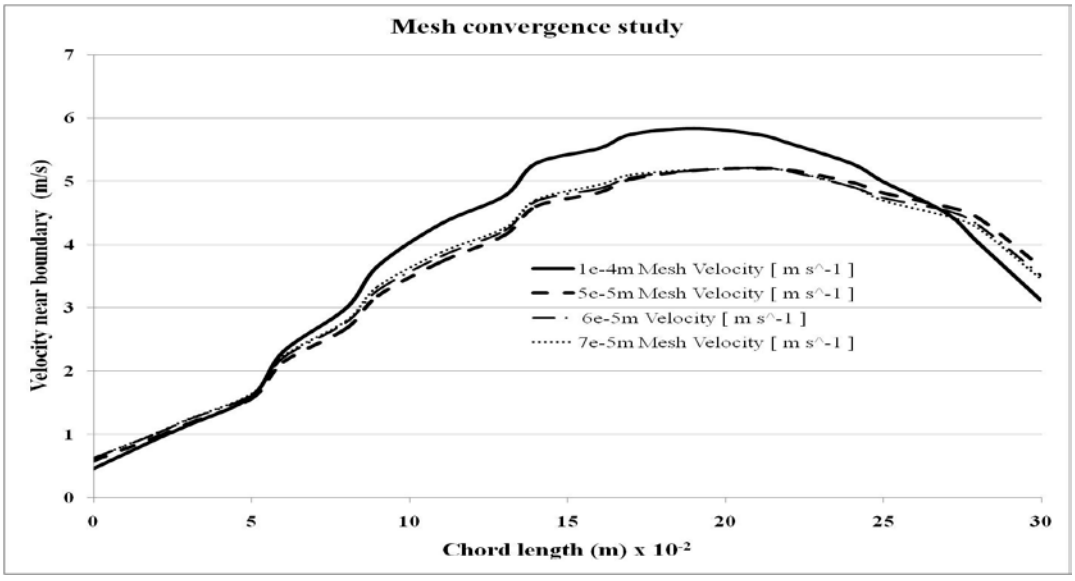


Figure 6. Mesh convergence/ grid convergence study

### 2.2.3 Mesh skewness and aspect ratio test

Skewness is one of the primary quality measures for a mesh. According to the definition of skewness, a value of 0 (zero) indicates an equilateral cell (best) and value 1 (one) indicates a completely degenerate cell (worst). Figure 7 shows the skewness of meshes which falls within the limits from 0.7 to 1.

The mesh orthogonality test which involves the angle between the vector that joins two mesh nodes and the normal vector for each integration point surface (n) associated with that edge. Figure 8 shows the result and it is also within the limits.

The cell aspect ratio is shown in figure 9 and it ranges from 1 to 40. The limit is an acceptable range for the simulation of the Ansys result.

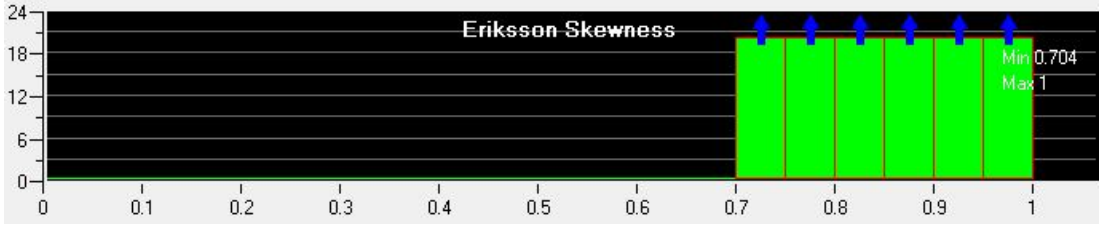


Figure 7. Mesh skewness test

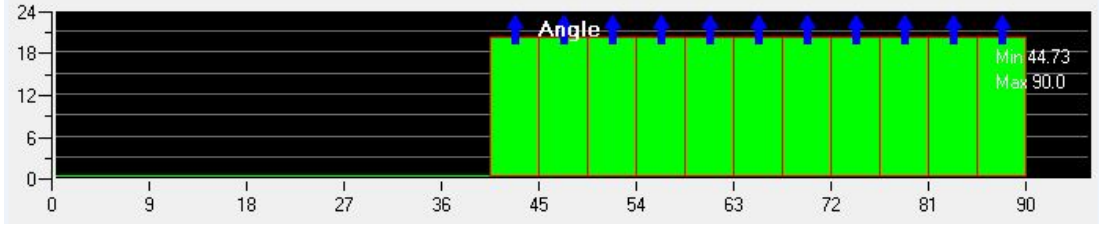


Figure 8. Mesh orthogonality test

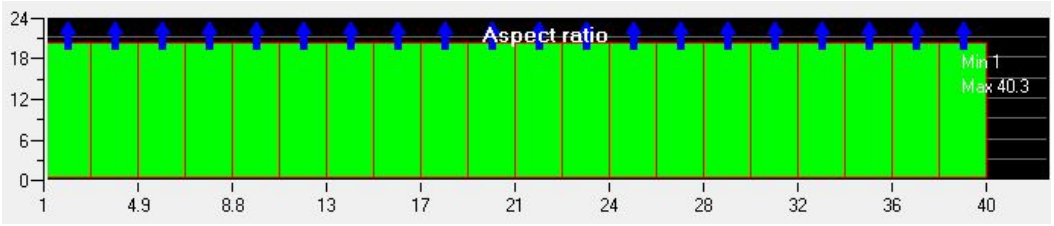


Figure 9. Mesh aspect ratio test

### 2.2.4 Flow solver

Commercially available ANSYS Fluent R15.0 is used to solve the above equations. The solver used is based on collocated methodology. It uses finite volume discretization technique to solve the equations. Gradients are calculated using Green-Gauss cell based methodology proposed by Holmes and Connel [32] and Rauch et al. [33].

Convection terms in the momentum equation are discretized using the second order upwind methodology.

In the second order upwind, quantities at cell faces are computed using a multi-dimensional linear reconstruction approach proposed by Barth and Jespersen [34]. The solution convergence criterion for the tested CFD models is a maximum residual of $10^{-5}$.

## 3. RESULTS AND DISCUSSIONS

### 3.1 Analysis of the velocity contours

The velocity contours obtained from CFD simulations of the corrugated triangular peak airfoil (model 1) and corrugated curved peak airfoil (model 2) of the chord Reynolds number 35000 and angles of attack (AOA) ranging from -4° to 12° are shown in figure 10 below.

The velocity contours of model 1 and model 2 at all simulated AOA were found almost equal and there is no significant variation in velocity contours at -4 AOA. However, at higher AOA, a significant velocity variation is observed in corrugated peak airfoil model 2.

High velocity is observed as and when flow touches the peak of the first corrugation. At AOA $-4^0$, the velocity at lower surface is higher in both models which show the negative lift and in agreement with the theory of lift.

At all positive AOA (0° to 12°), the velocity of the upper surface of the airfoil is significantly higher in both models.

However, in curved peak model 2, the velocity gradient is much higher than the triangular peak model 1 and also the area of the velocity difference in model 2 is significantly greater than for model 1.

The velocity accelerates due to sharp edge of the peak of corrugation. It is also found that in case of model 2, the boundary layers are much smaller than in case of model 1 so the flow of model 2 airfoil will separate after model 1.

### 3.2 Analysis of velocity vectors and vortices

The flow pattern of the triangular peak airfoil model 1 shows that the leading edge vortex (LEV) is trapped inside the valley with low velocity clockwise flow (Fig. 11). However, the LEV is not observed in curved peak model 2 as shown in figure 12.

This is due to non existence of the sharpness of the peak in this model. The velocity vortex core of model 1 is found and shown in figure 13, the first valley velocity vortex core is zoomed and shown in figure 14.

By observing figure 14, it is clear that the vortex is formed in the first valley with clockwise circulation and also boundary layers were present near the surface of the corrugation. By observing the boundary layers, the velocity gradient (du/dy) near the bottom of the valley is much more than in the top of the valley.

Corrugated triangular peak airfoil (model 1)

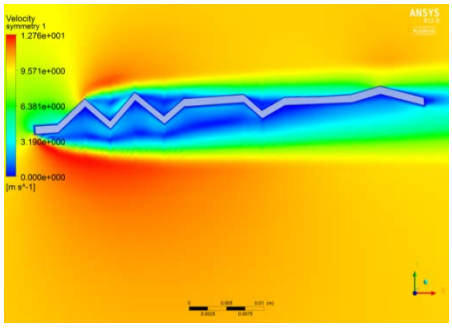


At angle of attack -4 degree

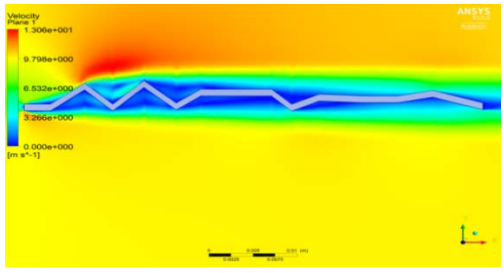


At angle of attack 0 degree

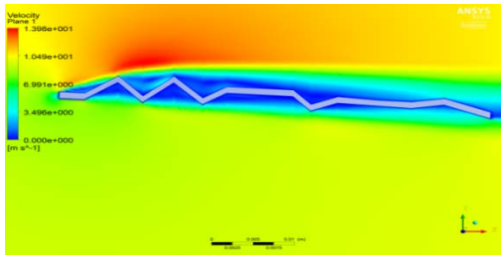


At angle of attack 4 degree

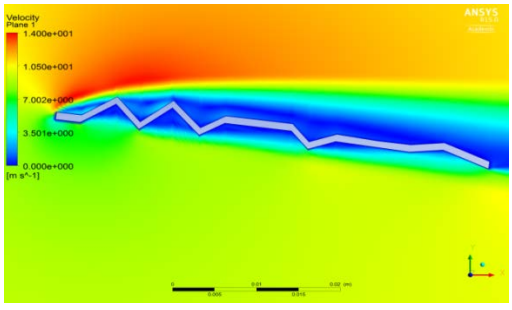


At angle of attack 8 degree

Corrugated curved peak airfoil (model 2)

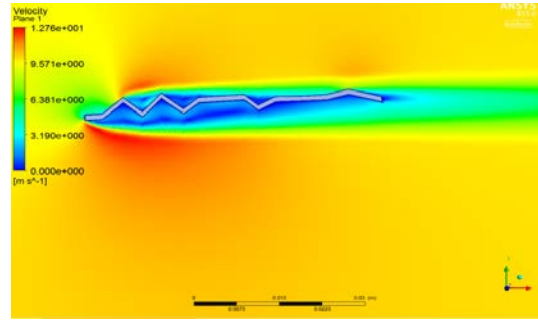


At angle of attack -4 degree

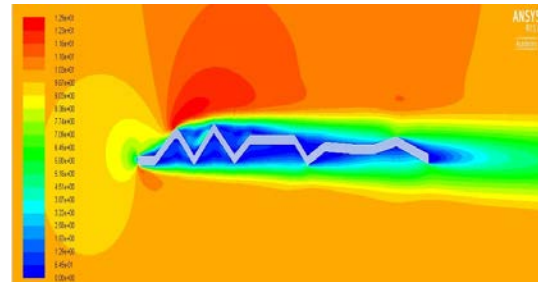


At angle of attack 0 degree

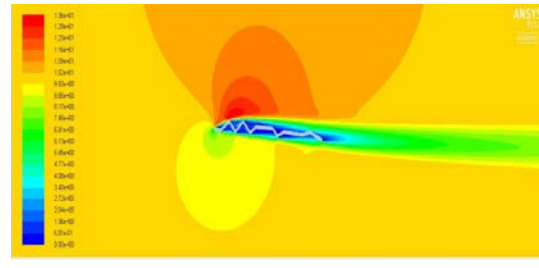


At angle of attack 4 degree

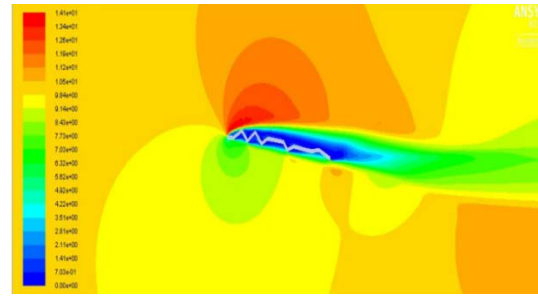


At angle of attack 8 degree

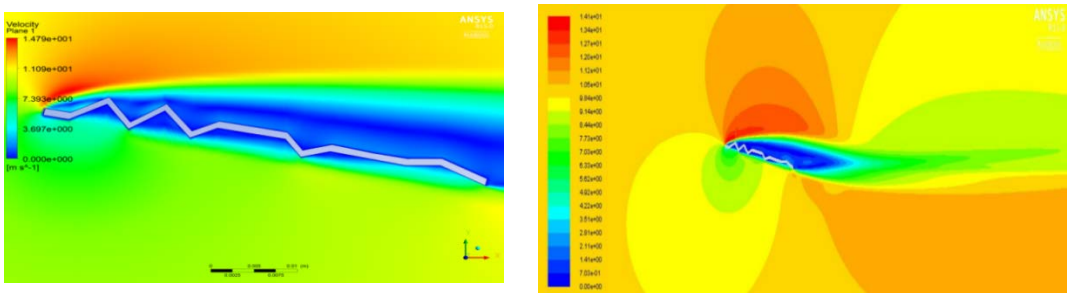

At angle of attack 12 degree At angle of attack 12 degree

Figure 10. Velocity contours at different angles of attack at Re 35000

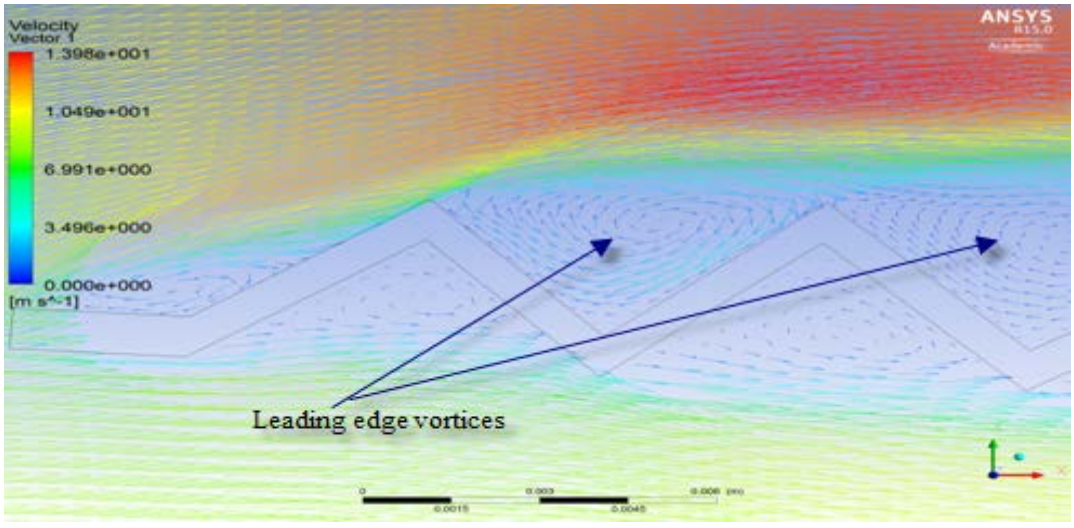


Figure 11. Velocity vector of traingular peak airfoil model 1 at 4 AOA and Re 35000

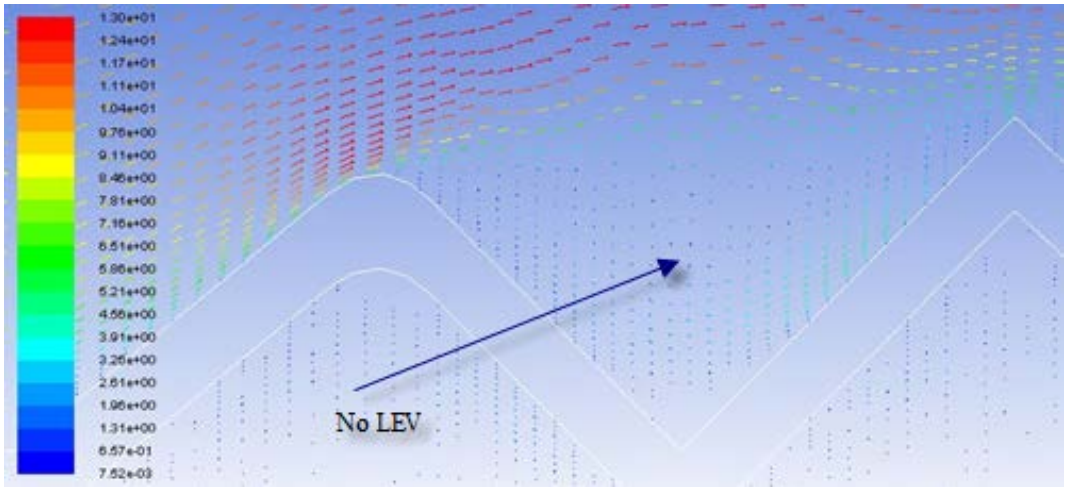


Figure 12. Velocity vector of curved peak airfoil model 2 at 4 degree AOA and Re 35000

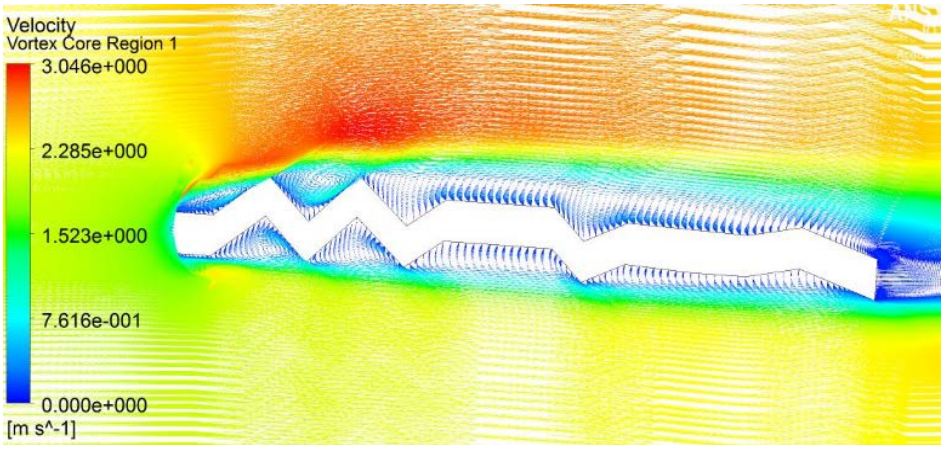


Figure13. Vortex core region of model 1 at 4 degree AOA and Re 35000

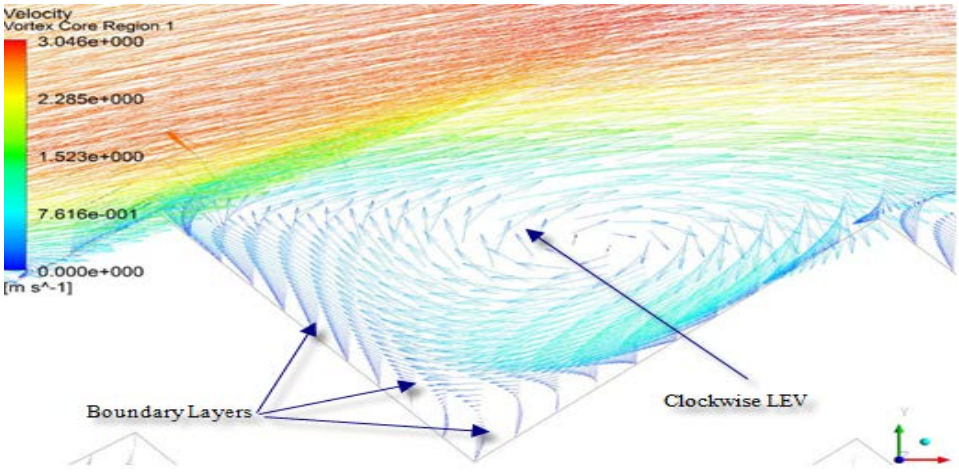


Figure 14. Zoomed view of vortex core of model 1at 4 degree AOA and Re 35000

### 3.3 Aerodynamic force analysis

The aerodynamic parameters such as lift force, drag force and aerodynamic performance parameters (L/D ratio) of the triangular peak model 1 and curved peak model 2 were obtained by simulation and the values of these parameters are shown in table 1 and 2, respectively. The plots of the aerodynamic forces like lift and drag against angles of attack and aerodynamic performance (L/D) against angles of attack are shown in Figure 15 and 16 respectively. The lift and drag of model 1 is higher than the model 2 upto 6 degree AOA. Above 6 degree AOA, the lift and drag of model 2 is increased more than the model 1. The aerodynamic performance of model 2 is found 4.5% higher than for model 1 at 4°AoA. This angle of attack (4 degree) is best suited for gliding of the model 2 wing, which gives low sink rate with high range and endurance.

Table 1. Aerodynamic Lift and Drag of model 1

| S. No | AoA | Lift (N) | Drag (N) | L/D |
|---|---|---|---|---|
| 1 | -4 | -0.73729 | 0.3115 | -2.366 |
| 2 | 0 | 0.792455 | 0.2757 | 2.8736 |
| 3 | 4 | 2.19238 | 0.3144 | 6.9723 |

| | | | | |
|---|---|---|---|---|
| 4 | 8 | 2.86312 | 0.4462 | 6.4158 |
| 5 | 12 | 3.122 | 0.6199 | 5.0362 |

Table 2. Aerodynamic Lift and Drag of model 2

| S. No | AoA | Lift (N) | Drag (N) | L/D |
|---|---|---|---|---|
| 1 | -4 | -0.72714 | 0.5261 | -1.3821 |
| 2 | 0 | 0.8065 | 0.2396 | 3.4036 |
| 3 | 4 | 2.0376 | 0.2791 | 7.3006 |
| 4 | 8 | 2.9723 | 0.50162 | 5.9254 |
| 5 | 12 | 3.2175 | 0.7871 | 4.0875 |

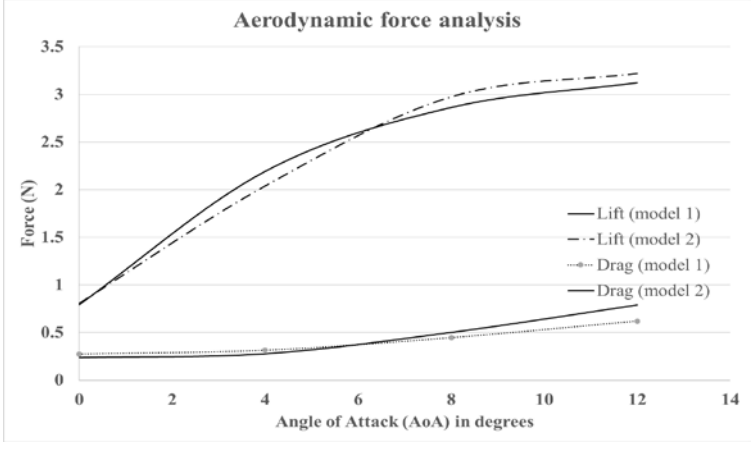


Figure15. Aerodynamic forces verses AOA at Re 35000 of model 1 and model 2

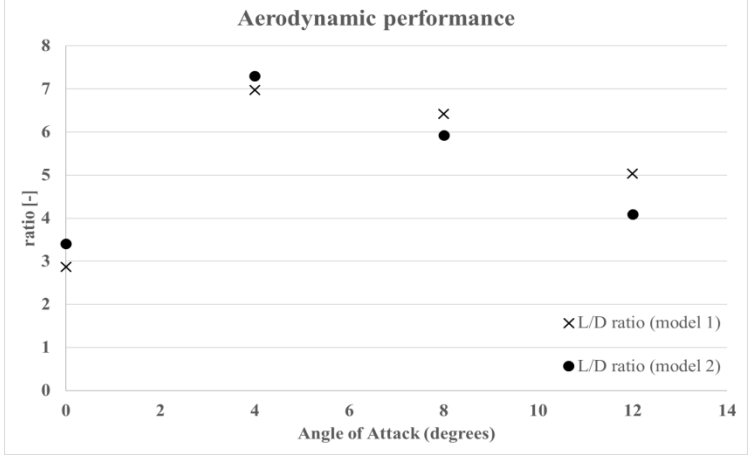


Figure 16. Comparison of Aerodynamic of model 1 and model 2

### 3.4 Validation of computational work

The present simulated velocity vortex core contour of the triangular peak model 1 is compared with the experimental work of Tamai et al. [22]. Tamai et al. [22] used the PIV measurement technique to measure the instant velocity and vortex core as shown in figure 17 (b). Present computational vortex core is shown in figure 17 (a). Both works are compared at 8 degree

AOA and Re 35000. Both figures show the LEVs in first and second corrugated valleys and also the high velocity range expands upto 40% of the chord length. The results of figure 17 (a) and (b) agreed with each other and the flow results are pretty close to each other. The present computational work which is undertaken at Re 35000 to find aerodynamic force coefficients ($C_L$ and $C_D$) is compared with the experimental work of Kesel, 2000 [20], which was conducted at Re 10000. The present computational results are very close to the experimental work of Kesel with 10% over pridicteded as shown in Fig. 18. It may be due to differfent tested Reynolds number of the present computational work which was performed at 35000 while Kesel's work was done at Re 10000.

## 4. CONCLUSIONS

The velocity contours for both models are almost the equal at low angles of attack. The high velocity on upper surface of the model 2 increases more than the model 1 in higher angles of attack (> 4 degree). So the lift forces of model 2 are 3% higher than in case of model 1 at higher AOA (> 4 degree). The aerodynamic performance of the curved peaked wing (model 2) is found to be higher by 4.5% as compared to the triangular peaked (model 1) at lower angle of attack (< $4^0$). Above $4^0$ AOA, the triangular peak model 1, performed better than the curved peaked model 2. The higher value of L/D ratio gives better gliding capability, high range and endurance and better sink rate of the corrugated wing with curved peak at low AOA (< $4^0$). The velocity and pressure contours showed no substantial difference in the flow behavior. The contours also showed that the leading edge velocity varies as the angles of attack increases, which tends to vary the pitching moments. Hence, the curved peak (model 2) is found better at the cruise condition of the flying.

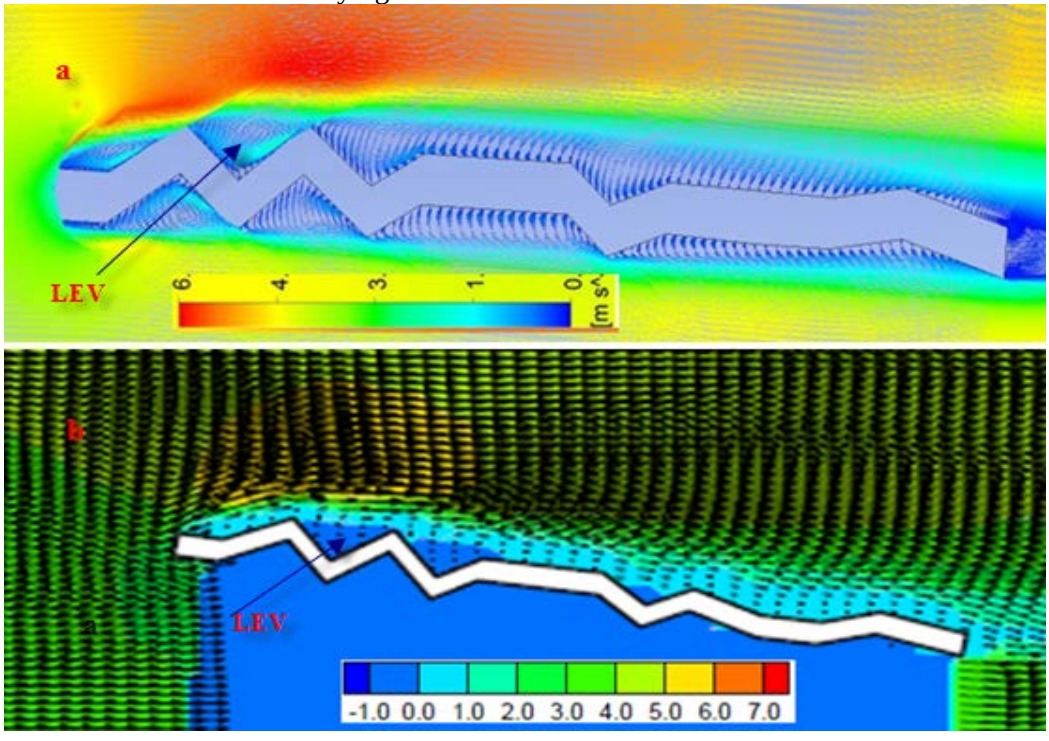


Figure 17. (a) Computational velocity vortex core of present work, (b) PIV measurement at 8 degree angle of attack at Re 35000 [22]

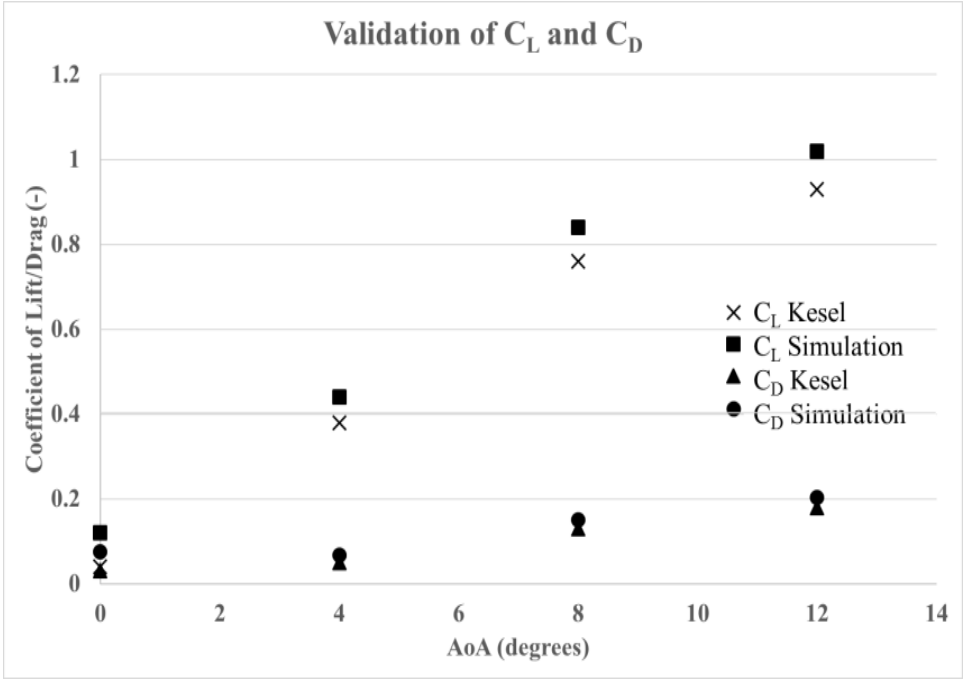


Figure 18. Validation of $C_L$ and $C_D$ with result of Kesel [16]

## REFERENCES

[1] E. Hankin, *The soaring flight of dragonfly*, In Proc. Camb. Phil. Soc., 1921.
[2] A. K. Brodsky, *The evolution of insect flight*, Oxford Press, 1994.
[3] J. Wakeling and C. P. Ellington, Drgonfly flight. I. Gliding flight and study state aerodynamic forces, *Journal of Experimental Biology*, **200** (3): 543-556.
[4] A. Vargas, R. Mittal, and H. Dong, A computational study of the aerodynamic performance of a dragonfly wing section in gliding flight, *Bioinspiration & biomemetics*, **3**(2):026004. Doi: 10. 1088/ 1748-3182/3/2/026004, 2008.
[5] R. J. Wootton, Functional morphology of insect wings, *Annual review of entomology*, **37** (1): 113-140, https://doi.org/10.1146/annurev.en.37.010192.000553, 1992.
[6] C. J. C. Rees, Form and function in corrugated insect wings, *Nature*, **256**: 200–203, 1975a.
[7] C. J. C. Rees, Aerodynamic properties of an insect wing section and a smooth aerofoil compared, *Nature* **258**: 141–142, 1975b.
[8] B. G. Newman, Model test on a wing section of an Aeschna dragonfly, *Scale effects in Animal Locomotion*, **35**: 280-285, 1997.
[9] D. J. S. Newman and R. J. Wootton, An Approach to the Mechanics of Pleating in Dragonfly Wings, *Journal of Experimental Biology*, **125**: 361-372, 1986.
[10] R. Rudolph, Aerodynamic properties of Libellula quadrimaculata L. (Anisoptera: Libellulidae), and the flow around smooth and corrugated wing section models during gliding flight, *Odonatologica*, **7** (1): 49-58, 1978.
[11] R. Buckholz, The functional role of wing corrugations in living systems, *Journal of Fluid Engineering*, **108** (1): 93-97, doi.org/10.1115/1.3242550, 1986.
[12] C. P. Ellington, The aerodynamics of hovering insect flight. I. The quasi-steady analysis, *Philosophical Transactions of the Royal Society of London. Series B, Biological Sciences*, **305** (1122): 1-15, https://www.jstor.org/stable/2396072 ,1984.
[13] C. P. Ellington, The aerodynamics of insect flight. II. Morphological parameters, *Phil. Trans. R. Soc. Lond. B*, **305** (1122): 17-40, https://www.jstor.org/stable/2396073, 1984.
[14] C. P. Ellington, et al., Leading-edge vortices in insect flight, *Nature*, **384**(6610): 626-630, https://doi.org/10.1038/384626a0, 1996.

[15] M. Okamoto, K. Yasuda and A. Azuma, Aerodynamic characteristics of the wings and body of a dragonfly, *J. Exp. Biology*, **199**: 281-294, PMID: 9317808, 1996.
[16] A. B. Kesel, Aerodynamic characteristics of dragonfly wing sections compared with technical aerofoil, *J. Exp. Biol*., **203**: 3125–3135, doi.org/10.1016/S0010-4825 (98)018-3, 2000.
[17] W. H. Ho and T. H. New, Unsteady numerical investigation of two different corrugated airfoils, Proceedings of the Institution of Mechanical Engineers, *Part G: Journal of Aerospace Engineering*, Volume: **231** issue: 13, page(s): 2423-2437, doi: 10.1177/ 09544100 16682539, 2016.
[18] W. H. Ho and T. H .New, CFD analysis of bio-inspired corrugated airfoils. In: 11th International Conference of Fluid Dynamics, Alexandria, Egypt Dec 2013.
[19] Y. D. Dwivedi, W. H. Ho, D. Jagadish, P. M. V. Rao, Spanwise Flow Analysis of Gliding Bio-inspired Corrugated Wing, *Journal of Advanced Research in Dynamical & Control Systems*, **12**-Special issue, 312-322, 2017.
[20] Y. D. Dwivedi, V. Bhargava, P. M. V. Rao and D. Jagadish, Aerodynamic Performance of Micro Aerial Wing Structures at Low Reynolds Number, *INCAS Bulletin*, **11** (1):107-120, doi: 10.13111/2066-8201.2019.11.1.8, 2019.
[21] Y. D. Dwivedi, and Y. B. Sudhir Sastry, An experimental flow field study of a bio-inspired corrugated wing at low Reynolds number, *INCAS Bulletin*, **11** (3), 55-65, doi: 10.13111/2066-8201.2019.11.3.5, 2019.
[22] M. Tamai, Z. Wang, G. Rajagopalan, H. Hu, and G. He, Aerodynamic Performance of a Corrugated Dragonfly Airfoil Compared with Smooth Airfoils at Low Reynolds Numbers, In: *45th AIAA Aerospace science meeting and Exhibits*, doi:10.2514/6.2007-483, 2007.
[23] A. Obata & S. Sinohara, Flow visualization Study of the aerodynamics of modeled dragonfly wings, *AIAA Jornal*, **47** (12). 3043-3046, doi :10.2514/1.43836, 2009.
[24] Y. H. Chen and M. Skote, Gliding performance of 3-D corrugated dragonfly wing with spanwise variation, *Journal of Fluid and Structures*, **62**: 1-13, doi: 10.1016/j.jfluidstructs, 2015.
[25] S. Gaurav and K. K. Jain, Numerical investigation of fluid flow and aerodynamic performance of a dragonfly wing section for micro air vehicles (MAVs) application, *Int. J. Innovat Scient Res*, **92**: 285–292, doi: 10.1.1.680.3222, 2014.
[26] K. Hord and Y. S. Lian, Numerical investigation of the aerodynamic and structural characteristics of a corrugated airfoil, *Journal of Aircraft*, **49**(3): 749-757, doi.org/ 10.2514/ 1.C031135, 2012.
[27] M. Kwok and R. Mittal, *Experimental investigation of the aerodynamics of a modeled dragonfly wing section*, Proceedings of AIAA Region-I MA Students Conference, doi: 10.1155/2017/3019640, 2005.
[28] H. Hu and, M. Tamai, Bio-inspired corrugated airfoil at low Reynolds numbers, *J Aircraft*, **456**: 2068–2077, doi: 10.2514/1.37173, 2008.
[29] D. E. Levy and A. Seifert, Simplified dragonfly airfoil aerodynamics at Reynolds numbers below 8000, *Phys Fluids*, **21**: doi.org/10.1063, 2009.
[30] D. E. Levy and A. Seifert, Parameter study of simplified dragonfly airfoil geometry at Reynolds number of 6000, *J. Theoretical Biology*, **266**(4):691–702, doi.org/10.1016/j.jtbi. 2010.07.016, 2010.
[31] T. H. New et al, Effects of corrugated aerofoil surface features on flow-separation control, *AIAA Journal* **521**:206–211, doi:10.1016, 2014.
[32] D. Holmes and S. Connell, Solution of the 2D Navier- Stokes equations on unstructured adaptive grid. American Institute of Aeronautics and Astronautics, In: *9th CFD conference*, 89-1932-CP, doi: 10.2514/6.1989-1932 1989.
[33] R. D. Rausch, J. T. Batina, and H. T. Y.Yang, Spatial adaptation procedures on unstructured meshes for accurate unsteady aerodynamic flow computation, **91**: doi: 10.2514/6.1991-1106, 1991.
[34] T. J. Barth and D. C. Jespersen, The design and application of upwind schemes on unstructured meshes, *AIAA paper 89-036*, 1989.